Thermochimica Acta, 139 (1989) 157–168
Elsevier Science Publishers B.V., Amsterdam – Printed in The Netherlands

HEAT CAPACITY STUDIES OF PHASE TRANSITIONS IN LANGBEINITES. I. $K_2Mn_2(SO_4)_3$ *

JULIANA BOERIO-GOATES **, BRIAN F. WOODFIELD, and JOHANNE I. ARTMAN
Department of Chemistry, Brigham Young University, Provo, UT 84602 (U.S.A.)
(Received 1 June 1988)

ABSTRACT

Heat capacity measurements have been made on two samples of $K_2Mn_2(SO_4)_3$. Both samples exhibit the phase change near 191 K which has been reported by other investigators as well as several additional heat capacity maxima. The temperatures and relative intensities of the peaks in each heat capacity curve depend significantly upon sample characteristics. One sample, which contained a small trace of water, exhibited peaks of approximately equal height at 182.9, 190.1 and 194.5 K, while the second sample, which also contained a small amount of water as well as some unreacted starting materials, had a very prominent first-order peak at 190.9 K and two minor peaks near 170 and 175 K. The possibility that these high precision heat capacity measurements reveal previously undiscovered phase transitions is being considered. Such transitions could indicate that $K_2Mn_2(SO_4)_2$ has been incorrectly classified as a Group II langbeinite rather than a Group I langbeinite. This conclusion is strengthened by the observation of multiple phase transitions in $K_2Mg_2(SO_4)_2$ as well.

INTRODUCTION

A series of compounds with the general formula $(M^+)_2(M^{2+})_2(SO_4)_3$ and the generic name langbeinites have been of interest because of the sequence of transitions to ferroelectric and/or ferroelastic phases which are observed as the materials are cooled from the paraelectric/paraelastic high temperature phase. Numerous compounds with this structure have been synthesized. Most langbeinites have cubic structures (space group $P2_13$) at room temperature [1], but two types of phase behavior have been observed as the temperature is lowered. Langbeinites classified as Group I [2] compounds undergo the following series of transitions [2]

$$\text{Cubic} \rightarrow \text{monoclinic} \rightarrow \text{triclinic} \rightarrow \text{orthorhombic} \quad (1)$$

* Dedicated to Professor E.F. Westrum, Jr., on the occasion of his 70th birthday and in honour of his contribution to calorimetry and thermal analysis.
** To whom correspondence should be addressed.

0040-6031/89/$03.50

as the temperature is lowered, while Group II langbeinites exhibit a single transformation to an orthorhombic (space group $P2_12_12_1$) structure [3–5] at lower temperatures. The phase transitions in these materials have been studied by group theoretical [6,7], spectroscopic [8–10] and diffraction methods [3–5], and by dielectric constant [3,11,12] and birefringence [12,13] measurements to ascertain the transition mechanism. All this work has not completely resolved questions concerning the driving force for these transitions, however.

The class of Group II langbeinites includes the following members of the potassium series: $K_2Cd_2(SO_4)_3$ [3], $K_2Ca_2(SO_4)_3$ [1], and $K_2Mn_2(SO_4)_3$ [11]. For two potassium compounds, $K_2Mg_2(SO_4)_3$ [11] and $K_2Ni_2(SO_4)_3$ [14], no transitions have yet been reported; $K_2Zn_2(SO_4)_3$ [11] and $K_2Co_2(SO_4)_3$ [15] are believed to be Group I langbeinites, although not all of the transitions in the sequence (1) have been observed. We have begun a study of the heat capacity of selected potassium langbeinites in order to shed more light on the mechanism responsible for the phase transitions observed in these materials. To date, only two calorimetric studies [13,16], both using differential scanning techniques, have been reported on potassium langbeinites. In this paper we report the results of our heat capacity measurements employing an adiabatic calorimeter, a method with higher precision than DSC, from 15 to 340 K on the manganese analogue $K_2Mn_2(SO_4)_3$. Our discovery of previously unreported transitions in the magnesium compound $K_2Mg_2(SO_4)_3$ will be published elsewhere [17].

EXPERIMENTAL

The $K_2Mn_2(SO_4)_3$ sample was prepared by slow evaporation of a hot aqueous solution containing stoichiometric quantities of K_2SO_4 and $MnSO_4$ (reagent grade from J.T. Baker and Co.) according to the methods described in ref. 11. After the solution had been concentrated to about half its initial volume over the course of a week, $K_2Mn_2(SO_4)_3$ crystals were filtered, ground, and dried in vacuo. A $BaSO_4$ gravimetric analysis yielded a value of 60.21 ± 0.22 wt.% of sulfate in the product; the theoretical value is 60.51. Further characterization by the technique of proton-induced X-ray emission (PIXE) analysis gave results for the K/S, K/Mn and S/Mn mass ratios of 0.807 ± 0.016 (0.813), 0.709 ± 0.014 (0.712), and 0.881 ± 0.018 (0.875), respectively; the uncertainties given are an estimate of 2σ, while the theoretical values are cited in parentheses. Inspection of the material under a polarizing microscope and by powder X-ray diffraction showed no signs of contamination by the non-isotropic starting materials.

A portion of the $K_2Mn_2(SO_4)_3$ sample weighing 57.1037 g (0.11990 moles) was loaded into a gold-plated copper calorimeter which was then evacuated and sealed under an atmosphere of 4.533 kPa of helium exchange gas. Apiezon-T grease was used to enhance the thermal conductivity at the interfaces between the calorimeter surface and the thermometer and thermocouples. The details of the calorimeter and the loading procedure have been published previously [18]. The contributions of the empty calorimeter, grease, helium and thermometer to the total measured heat capacity ranged from 25% at 20 K to 35% from 50–300 K. A Leeds and Northrup 25 Ω capsule-type platinum resistance thermometer calibrated on the IPTS-68 temperature scale was used to measure temperatures.

The automated adiabatic cryostat used in this study is essentially the modified-Westrum design described previously [18], although several changes have been made to the cryostat and instrumentation since the publication of the description of our original apparatus. These include replacing the home-built temperature controller for the main adiabatic shield with commercial electronics and measuring the calorimeter temperature using the Solartron DVM in the D.C. Volts mode rather than the True Ohms mode as earlier reported. The modifications will be discussed in detail in another publication [17].

RESULTS

The heat capacities obtained in this study are reported in Table 1 in chronological order. The approximate size of the temperature increment used in each measurement can be inferred from the temperature differences between successive entries in a series. A plot of the heat capacity measurements is shown in Fig. 1 with data from series 4 and 10 omitted for clarity.

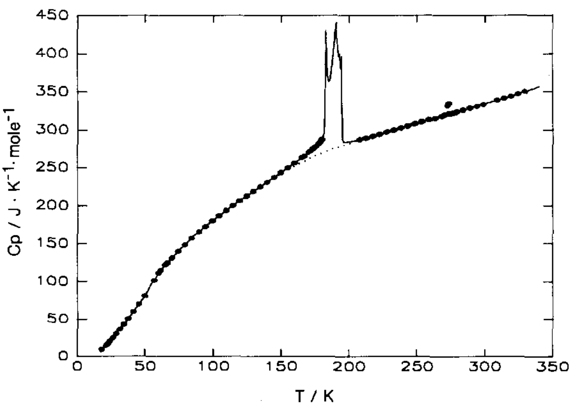

Fig. 1. The heat capacity of $K_2Mn_2(SO_4)_3$ as a function of temperature. The solid line represents the smoothed curve through the data points, while the dotted line represents the estimation of the lattice heat capacity. The experimental data has been omitted from the transition region for clarity.

TABLE 1

Results of the heat capacity measurements on $K_2Mn_2(SO_4)_3$

T (K)	C_p ($J K^{-1} mol^{-1}$)	T (K)	C_p ($J K^{-1} mol^{-1}$)	T (K)	C_p ($J K^{-1} mol^{-1}$)
Series 1		148.80	242.3	270.21	319.3
202.59	285.5	153.90	248.8	275.38	321.7
207.63	287.5	159.01	255.1	280.53	324.8
212.80	289.7	164.11	261.8	285.67	328.3
217.96	292.1	169.21	268.7		
		174.30	276.4	Series 11	
Series 2		179.37	290.0	280.73	324.4
201.82	285.3			285.87	326.7
206.87	287.2	Series 7		291.03	329.3
212.03	289.3	182.46	370.2	296.17	332.0
217.20	291.9	183.46	402.5	301.30	334.9
222.36	294.6	184.50	369.0	306.43	337.5
227.52	297.4	185.57	369.9	311.56	340.3
		186.60	379.8	316.69	342.7
Series 3		187.62	396.4	321.83	345.3
232.97	299.8	188.62	412.0	326.97	348.4
238.12	302.5	189.63	429.6		
243.28	305.1	190.66	426.3	Series 12	
248.44	307.7	191.72	403.8	295.43	331.5
253.60	310.2	193.32	390.2	300.58	334.1
258.76	312.7	195.66	289.3	305.72	336.6
263.93	315.3	197.99	283.9	310.86	339.3
269.09	317.7	200.08	284.4	315.98	342.0
274.25	320.2	202.16	285.1	321.11	344.5
		204.24	286.0	326.24	347.7
Series 4		206.31	286.9		
275.05	320.2			Series 13	
280.08	322.6	Series 8		196.13	297.5
285.24	325.2	304.55	337.0	201.20	284.9
290.41	327.5	309.68	340.1	206.45	287.0
295.58	329.8	314.83	341.7	211.62	289.1
300.74	332.1			216.78	291.6
305.90	334.5	Series 9		221.95	294.4
311.06	336.8	319.97	344.4	227.11	297.0
316.22	338.9	325.11	347.3	232.27	299.6
321.34	347.1	330.24	349.9	237.43	302.3
		335.37	353.1	242.60	305.1
Series 5		340.47	356.8		
316.69	342.3			Series 14	
321.90	345.2	Series 10		247.71	307.6
327.11	348.2	239.17	304.2	252.85	310.4
332.31	351.1	244.34	309.1	258.01	312.9
337.50	354.8	249.51	310.6	263.16	315.1
		254.68	314.8	268.30	317.9
Series 6		259.85	314.8	273.34	334.6
143.64	235.9	265.04	316.7	278.52	322.8

TABLE 1 (continued)

T (K)	C_p (J K^{-1} mol^{-1})	T (K)	C_p (J K^{-1} mol^{-1})	T (K)	C_p (J K^{-1} mol^{-1})
283.77	325.9	Series 21		Series 23	
288.92	328.4	109.20	193.4	166.85	264.6
294.07	330.9	114.15	200.0	172.17	272.3
		119.21	206.4	185.80	350.7
Series 15		124.28	212.7	197.37	284.1
298.74	333.3	129.36	218.9	199.05	284.5
308.99	338.9	134.45	224.9		
314.12	341.3	139.54	231.0	Series 24	
319.24	344.2	144.64	237.3	166.86	264.7
324.38	346.7	149.74	243.5	172.20	272.3
329.51	349.8	154.84	249.7	185.83	350.7
		159.94	256.1	197.41	284.2
Series 16		165.04	262.8	199.09	284.5
21.52	15.03	170.14	269.9		
22.76	17.34				
24.40	20.59	Series 22		Series 25	
		173.83	275.1	173.61	274.9
Series 17		175.43	277.7	175.21	277.7
26.51	25.05	176.46	279.7	176.25	279.4
28.87	30.29	177.50	281.7	177.29	281.2
31.33	36.09	178.54	284.3	178.32	283.6
34.07	42.74	179.57	287.6	179.36	286.5
		180.60	292.2	180.39	291.2
Series 18		181.62	307.5	181.16	296.9
37.32	50.69	182.57	383.2	181.68	307.0
41.07	59.80	183.52	400.6	182.06	322.0
45.23	69.89	184.57	369.2	182.30	360.0
49.66	80.83	185.64	369.9	182.55	380.8
		186.67	379.8	182.80	411.9
		187.68	395.7	183.05	423.9
Series 19		188.69	409.0	183.31	406.9
56.53	101.5	189.70	431.0	183.57	394.4
61.46	115.4	190.72	431.1	183.85	373.1
66.15	125.0	191.78	407.0	184.11	366.9
		192.84	398.9	184.37	365.2
Series 20		193.91	384.2	184.63	362.5
59.72	111.7	195.04	307.6	184.89	363.5
64.77	122.6	196.20	284.1	185.15	364.6
69.53	131.2	197.27	284.2	185.41	363.1
74.37	140.1	198.31	284.2	185.67	363.4
79.24	148.7	199.35	284.5	185.93	365.2
84.14	157.0	200.39	284.7	186.18	373.4
89.08	164.9	201.43	285.3	186.44	371.9
94.05	172.5	202.47	285.9	186.70	376.5
99.05	179.7	204.03	286.2	186.96	380.3
104.06	186.6	206.11	287.1	187.21	383.2

TABLE 1 (continued)

T (K)	C_p ($J\ K^{-1}\ mol^{-1}$)	T (K)	C_p ($J\ K^{-1}\ mol^{-1}$)	T (K)	C_p ($J\ K^{-1}\ mol^{-1}$)
Series 26		193.49	389.1	217.69	292.1
187.49	391.1	193.75	382.6	222.85	294.9
187.77	394.7	194.01	382.2	228.02	297.5
188.03	402.0	194.27	375.0	233.18	300.1
188.29	399.5	194.53	392.3	238.35	302.8
188.55	400.9	194.81	307.2	243.51	305.7
188.80	404.5	195.11	285.4	248.67	308.2
189.06	410.1				
189.31	420.3	Series 27		Series 29	
189.57	420.5	195.38	284.1	253.74	310.8
189.82	430.4	195.65	285.2	258.88	313.5
190.08	438.5	195.91	284.8	263.52	315.4
190.34	434.9	196.18	285.0	267.63	317.9
190.60	432.9	196.44	283.4	270.17	319.8
190.86	425.0	196.83	284.3	271.17	320.0
191.12	419.5	197.35	283.7	272.16	331.6
191.39	414.2	197.87	284.1	273.21	321.5
191.65	407.2	198.52	284.3	274.26	321.0
191.91	406.7	199.31	284.2	275.30	321.7
192.18	400.4			276.33	321.9
192.44	396.2	Series 28		277.36	322.2
192.70	396.2	202.25	285.2	279.43	323.8
192.96	398.5	207.36	287.3	283.56	326.3
193.22	396.5	212.53	289.5	288.70	329.0

A slight amount of irreproducibility was observed in the initial sets of measurements above 220 K, but consistent results were obtained after series 13. Concurrent with the ability to reproduce the heat capacity curve was the appearance of a small anomaly in the vicinity of the ice point (see series 13–14 and series 28 and 29). From the magnitude of the excess enthalpy in this region, we have been able to estimate the amount of water in the sample to be less than 0.02 mass%. The measured sample mass was adjusted for this quantity of water, but corrections for the heat capacity of water were negligible outside the fusion region.

The most prominent feature of the heat capacity measurements is the anomaly in the region of 190 K where other investigators [11,12] have reported the existence of a first-order transition. An enlarged view of the region near 190 K, which illustrates the details of the transition heat capacity, is given in Fig. 2. Data points taken with temperature increments greater than 2 K have been omitted from this drawing. The smooth curve drawn through the observed data points has been constructed keeping in mind that each experimental value represents the average heat capacity over the temperature increment of the measurement. In regions of sharp curva-

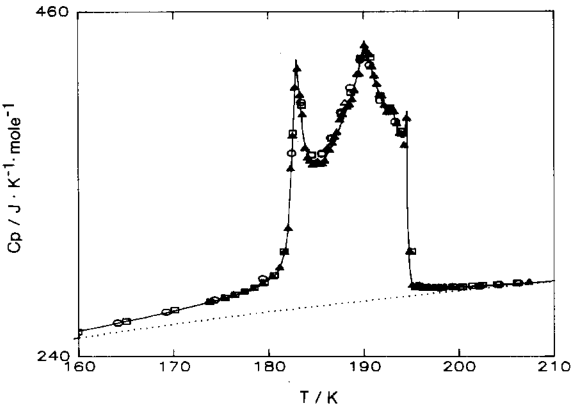

Fig. 2. An enlarged view illustrating the details of the transition region in $K_2Mn_2(SO_4)_3$. The symbols correspond to data from different series: ○, series 6, 7; □, series 22; and ▲, series 25–27.

ture, therefore, the curve may not pass directly through points taken with large temperature increments. Also, points obtained with smaller temperature intervals are subject to increased relative error, and experimental uncertainties have been considered in generating the smooth curve which is

TABLE 2

Enthalpies of transition for $K_2Mn_2(SO_4)_3$

Data source	H(196.15 K) − H(180.00 K) (J mol^{-1})	H(220 K) − H(140 K) [a] (J mol^{-1})	S(220 K) − S(140 K) (J K^{-1} mol^{-1})
Series 6–7 [b]	5995	23146	
Series 22 [c]	6192	23343	
Series 25–27 [c]	5979	23130	
Series 23 [d]	6057	23208	
Series 24 [d]	6076	23227	
Numerical integration of C_p curve	5990	23141	129.2
Average	6048	23199	
Numerical integration of lattice C_p curve	4439	21336	119.5
Excess thermodynamic quantities		$\Delta H_t = 1863$	$\Delta S_t = 9.7$

[a] The enthalpy difference H(220 K) − H(140 K) has been calculated by adding 17151 J mol^{-1}, the additional enthalpy contribution for this larger temperature interval, to each entry under the second column.
[b] Measurements taken with increments of 2–5 K through the transition region.
[c] Measurements taken with increments of 0.25–2 K through the transition region.
[d] Single long heating run through the transition region.

consistent with the different series of data that cover this region. Numerical integration of the hand-drawn curve from 180 to 196.15 K yielded values for the enthalpy and entropy contributions in this region. This enthalpy can be compared with that obtained by summing the energy input from individual measurements in appropriate series. The agreement of these results, sum-

TABLE 3

Standard thermodynamic functions for $K_2Mn_2(SO_4)_3$; $T_r = 298.15$ K

T (K)	C_p^0 ($J\ K^{-1}\ mol^{-1}$)	$S^0(T)$ ($J\ K^{-1}\ mol^{-1}$)	$H^0(T) - H^0(T_r)$ ($J\ mol^{-1}$)	$-\{G^0(T) - H^0(T_r)\}/T$ ($J\ K^{-1}\ mol^{-1}$)
15	0.349	0.174	−64307	4287.3
20	12.557	1.536	−64281	3215.6
25	21.79	5.292	−64196	2573.1
30	32.94	10.227	−64060	2145.6
35	45.02	16.21	−63865	1840.9
40	57.19	23.01	−63610	1613.3
45	69.34	30.45	−63293	1437.0
50	81.76	38.39	−62916	1296.7
60	112.3	56.06	−61942	1088.4
70	132.1	74.93	−60715	942.3
80	150.0	93.76	−59304	835.1
90	166.4	112.4	−57720	753.7
100	181.0	130.7	−55982	690.5
110	194.6	148.6	−54104	640.4
120	207.4	166.1	−52094	600.2
130	219.7	183.2	−49958	567.4
140	231.3	199.9	−47702	540.6
150	243.9	216.3	−45325	518.4
160	256.4	232.4	−42823	500.0
170	269.5	248.3	−40195	484.8
180	289.4	264.2	−37418	472.1
190	437.0	284.1	−33735	461.6
200	284.6	301.6	−30334	453.2
210	288.4	315.9	−27399	446.4
220	293.5	329.4	−24490	440.7
230	298.5	342.6	−21531	436.2
240	303.7	355.4	−18520	432.6
250	308.9	367.9	−15456	429.7
260	313.9	380.1	−12342	427.6
270	318.8	392.1	−9179	426.1
280	324.0	403.7	−5966	425.0
290	329.2	415.2	−2699.6	424.5
300	334.2	426.4	617.5	424.4
320	344.4	448.3	7403	425.2
340	356.9	469.6	14409	427.2
273.15	320.4	395.8	−8173	425.7
298.15	333.3	424.4	0.000	424.4

marized in Table 2, indicates the reproducibility of the measurements and that the smooth curve is a reasonable representation of the true heat capacity. Comparison of the experimental data with the lattice curve shows that the excess heat capacity begins near 140 K and continues to 220 K; the contributions to the enthalpy from this additional region are included in the third column of Table 2.

Lacking sufficient thermal and spectroscopic data to calculate the background heat capacity, an estimate, shown as the dotted line in Figs. 1 and 2, has been obtained by a smooth interpolation of the data above and below the transition. Numerical integration of this estimated lattice heat capacity curve yielded the values for the lattice enthalpy and entropy shown in Table 2. The differences between the total and lattice enthalpies and entropies are the excess thermodynamic quantities which can be associated with effects arising from the transition.

Orthogonal polynomials have been fitted to the heat capacity data in regions where there is no contribution from transitions. Above 220 K, only the data from series 13, 14, 28 and 29 were used in the fitting process. From these polynomials and the quantities determined by numerical integration of the heat capacity curve in the transition region, thermodynamic functions have been generated at smooth temperatures and are reported in Table 3. Contributions to the thermodynamic functions below the lowest temperature of our measurements have been estimated assuming Debye behavior.

DISCUSSION

Several different mechanisms have been proposed to explain the transition in Group II langbeinites like $K_2Mn_2(SO_4)_3$. The possibility of a transition driven by a soft mode was predicted by Dvořák [6], yet no evidence for soft modes has been observed in spectroscopic studies of $K_2Mn_2(SO_4)_3$ [9] or $K_2Cd_2(SO_4)_3$ [8]. Yamada et al. [4] refined their X-ray diffraction data of $K_2Mn_2(SO_4)_3$ with sulfates disordered between two orientations in the high temperature cubic phase, and suggested that the transition arose from an ordering of the sulfate ions in the orthorhombic phase. In a more recent X-ray diffraction study of $K_2Mn_2(SO_4)_3$, however, Speer and Salje [5] found no significant improvement in the refinement by assuming disordered sulfate ions, nor did Abrahams et al. [3] find evidence for disorder in their very careful structural studies of the high temperature phase of $K_2Cd_2(SO_4)_3$. Speer and Salje have rejected an order–disorder mechanism as the explanation for the transition and propose instead that the transition arises from instabilities in the coordination spheres around the cations [5].

We had expected that our heat capacity measurements would provide some answers regarding the existence of disorder, since the excess entropy

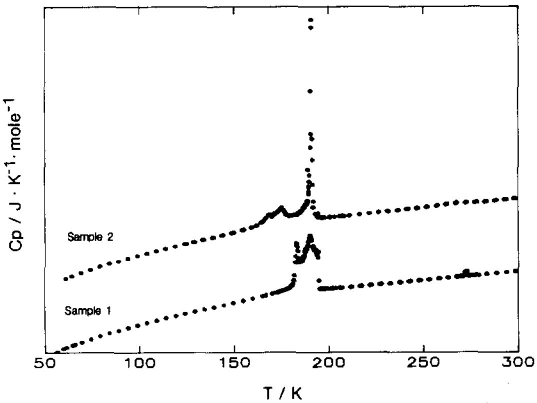

Fig. 3. A comparison of the heat capacities of two different samples of $K_2Mn_2(SO_4)_3$. The top curve which has been shifted by 200 J K^{-1} mol^{-1} is the heat capacity of sample 2; the bottom curve is the heat capacity of sample 1. Below 140 K and above 220 K the heat capacities of the two samples are in good agreement.

which can be obtained from these measurements is often on the order of $R \ln(N_2/N_1)$ where N_2 and N_1 refer to the number of allowed orientations in the high and low temperature phases, respectively. A value of $R \ln 2$ (5.76 J K^{-1} mol^{-1}) would be expected for ΔS_t if two-fold disorder were present, while our measurements yield a number which is closer to $R \ln 3$ (Table 2). However, the interpretation of the magnitude of our excess entropy is hindered by the presence of the multiple peaks in the C_p curve. The set of peaks we observe at 182.9, 190.1, possibly 193.1, and 194.5 K is an indication that more than one transition has taken place in the sample, yet no reports of a sequence of phase transitions in $K_2Mn_2(SO_4)_3$ have been made heretofore. The question then becomes whether the results arise from an artifact of our sample, perhaps from inhomogeneities in the sample stoichiometry or strain induced during the process which occurred above 220 K associated with the development of the water-fusion peak, or $K_2Mn_2(SO_4)_3$ is actually a Group I compound.

Measurements we performed on a second sample of $K_2Mn_2(SO_4)_3$ which contained several percent of the unreacted sulfates present some additional information relating to this question. Plots of the results from the two $K_2Mn_2(SO_4)_3$ samples are given in Fig. 3. Several significant differences between the heat capacities of the two specimens were observed, although the agreement is good below 140 K and above 220 K. The second sample showed reproducible heat capacities above 220 K, with the only evidence for water contamination being a slight change in curvature of the heat capacity near the water-fusion region. Moreover, the first-order character of the transition at 190.9 K was readily apparent in this sample, since the heat capacity rises much more steeply. Two additional peaks, at 170 and 175 K, are also found in the heat capacity of this sample, however.

Each sample, then, displays at least three maxima in its heat capacity, but their characteristics are much different. The maxima in the first sample are closely spaced, and the heat capacity between the peaks remains quite high. In the second sample, the peak at 190.9 K predominates and is separated much better from the other peaks. However, the shape of the minor peaks are not as well-defined as in the first sample because of the relatively large temperature increments used in this region.

At this point, we can draw few hard conclusions concerning the origin of the multiple peaks, although it does not appear to be due to the presence of water since multiple peaks appear in sample two, where there is less evidence for water contamination. Nor does it appear likely that they arise from contamination of the sample by unreacted starting materials, since the additional transitions are minor in the sample which is known to be contaminated, and are more prominent in the sample with the better chemical purity.

Adiabatic calorimetry is one of the most sensitive techniques for detecting phase transitions, and it is very possible that the other techniques which have been used to study $K_2Mn_2(SO_4)_3$ have not had the resolution to detect closely-spaced transitions. Since Type I langbeinites eventually end up in an orthorhombic form, the possibility exists that $K_2Mn_2(SO_4)_3$ has been wrongly classified as a Type II langbeinite if the intermediate transitions were missed and only the final low temperature phase was detected.

Further support for this possibility comes from heat capacity measurements we have performed on $K_2Mg_2(SO_4)_3$ [17]. This sample was prepared from the melt, thereby avoiding problems with water contamination, and exhibited multiple transitions below 70 K. Our results are the first evidence for any phase transitions in $K_2Mg_2(SO_4)_3$. In fact, Speer and Salje [5] have predicted that no transition would occur in this material.

Measurement of the heat capacities of other Type II langbeinites using adiabatic calorimetry to search more closely for additional phase transitions in these compounds would be of interest. While DSC measurements of the phase transitions in $K_2Co_2(SO_4)_3$ [16] and $K_2Cd_2(SO_4)_3$ [9] have been made, this technique is frequently incapable [19] of resolving closely spaced transitions. Phase transformations in the compounds studied by this technique may have been undetected. Additional studies with $K_2Mn_2(SO_4)_3$ samples of high crystalline quality would also be worthwhile.

ACKNOWLEDGMENTS

We would like to acknowledge the assistance and encouragement provided over the years by Prof. Edgar F. Westrum, Jr. His provision of schematics for the cryostat and shield control units, in particular, helped to make this work possible. Financial support from the College of Physical and

Mathematical Sciences at Brigham Young University is gratefully acknowledged.

REFERENCES

1 H.F. McMurdie, M.C. Morris, J. de Groot and H.E. Swanson, J. Res. Natl. Bur. Stand., 75A (1971) 435.
2 T. Hikita, M. Kitabatake and T. Ikeda, J. Phys. Soc. Jpn., 49 (1980) 1421.
3 S.C. Abrahams and J.L. Bernstein, J. Chem. Phys., 67 (1977) 2146; S.C. Abrahams, F. Lissalde and J.L. Bernstein, J. Chem. Phys., 68 (1978) 1926; F. Lissalde, S.C. Abrahams, J.L. Bernstein and K. Nassau, J. Appl. Phys., 50 (1979) 845.
4 N. Yamada, M. Maeda and H. Adachi, J. Phys. Soc. Jpn., 50 (1981) 907.
5 D. Speer and E. Salje, Phys. Chem. Miner., 13 (1986) 17.
6 V. Dvořák, Phys. Stat. Sol. B, 52 (1972) 93.
7 V. Dvořák, Phys. Stat. Sol. B, 66 (1974) K87.
8 V. Devarajan and E. Salje, Phys. Chem. Miner., 13 (1986) 25.
9 S. Kreske and V. Devarajan, J. Phys. C: Solid State Phys., 15 (1982) 7333.
10 L.T. Latush, L.M. Rabkin and V.I. Torgashev, Ferroelectrics, 48 (1983) 247.
11 T. Hikita, S. Sato, H. Sekiguchi and T. Ikeda, J. Phys. Soc. Jpn., 42 (1977) 1656.
12 N. Yamada, Y. Chubachi and T. Ikeda, J. Phys. Soc. Jpn., 45 (1978) 1638.
13 V. Devarajan and E. Salje, J. Phys. C: Solid State Phys., 17 (1984) 5525.
14 T. Hikita, H. Sekiguchi and T. Ikeda, J. Phys. Soc. Jpn., 43 (1977) 1327.
15 N. Yamada, T. Hikita, M. Maeda and T. Ikeda, J. Phys. Soc. Jpn., 49 suppl. B (1977) 102.
16 B. Brezina and A. Fousková, Kristall Tech., 13 (1978) 623.
17 J. Boerio-Goates, B.F. Woodfield and J.I. Artman, to be submitted.
18 J. Boerio-Goates and B.F. Woodfield, Can. J. Chem., 66 (1988) 645.
19 M.A. White, Thermochim. Acta, 74 (1984) 55.